Characterization of Uniform Microstrip Line and Its Discontinuities Using the Time-Domain Method of Lines

S. NAM, HAO LING, MEMBER, IEEE, AND TATSUO ITOH, FELLOW, IEEE

Abstract—**The general formulation and the procedure of the time-domain method of lines for the analysis of wave scattering and propagation properties in a planar circuit are described. The results of the time-domain data and the derived frequency-domain characteristics for the uniform microstrip line and its several discontinuities (step, open-end, and gap) are presented.**

I. Introduction

AN ACCURATE full-wave analysis of a planar transmission line and its discontinuities becomes increasingly important for the design of microwave and millimeter-wave circuits as the operating frequency increases. This is because the quasi-static analysis is not valid in the high-frequency range and the time-consuming cut-and-try cycle cannot be used in the monolithic microwave integrated circuit. There are several full-wave approaches for obtaining the frequency-dependent parameters of a uniform transmission line and its discontinuities [1–5]. All of them are frequency-domain methods. Hence, if a pulsed signal is considered in a structure, the problem should be solved at many different frequencies to obtain data for a wide range of frequencies because a pulse contains a wide frequency spectrum. The time-domain analysis of microwave planar transmission structures provides an alternative to the frequency-domain approach [6]–[8]. It is useful for obtaining the characteristics of a uniform transmission line and for calculating the scattering parameters of its discontinuities for a wide range of frequencies as well as for studying the behavior of a pulsed signal in structures such as high-speed digital circuits. Usually, the space is discretized into three-dimensional mesh at which the field value is calculated so that a large memory and a long computation time are required.

Previously, the time-domain method of lines (TDML) was proposed as a new time-domain technique for the analysis of planar structures [9], in which the space is approximated by many lines located only at the two-dimensional discretization points on the substrate surface. Since an analytical solution can be found along each line, the memory and the computation time can be saved. However, the method has been applied only to two-dimensional problems to obtain the scattering data of the input pulse in the time domain and the cutoff characteristics in the frequency domain for planar transmission structures. In this paper, it is shown that the TDML can be extended to three-dimensional problems. The time-domain data for a planar transmission line and its discontinuities can be obtained by the TDML. From the time-domain results, the frequency-domain characteristics for a wide range of frequencies can be found by the Fourier transform. The results for a uniform microstrip line and its discontinuities (step-in-width, open-end, and gap) are presented and compared with available published data.

Manuscript received March 31, 1989; revised July 18, 1989. This work was supported by Cray Research, by the Office of Naval Research under Grant N00014-89-J-1006, and by the Texas Advanced Technology Program.

The authors are with the Department of Electrical and Computer Engineering, University of Texas at Austin, Austin, TX 78712.

IEEE Log Number 8930958.

II. Formulation and Procedure of the Method

Let us consider the general planar transmission line with discontinuity shown in Fig. 1. In order to apply the TDML, electric walls or magnetic walls need to be placed at both ends of the waveguide so that a resonant structure results. Fig. 2 shows the top view of the structure with discretization points for the y component of electric field, E_y. It is assumed that the structure has spatial symmetry in the x direction so that the problem can be reduced by a factor of 2.

A. Discretization

As shown in Fig. 2, the structure is discretized by many field lines, which are properly placed to satisfy the boundary conditions on the sidewalls and the end walls. For example, since the Neumann boundary condition for E_y is applied along sidewall A and the Dirichlet condition at sidewall B, the E_y points are located away from sidewall A by one half of Δx and away from sidewall B by one Δx. It is known that the edge of the microstrip should be located around $\Delta x/4$ in Fig. 2 to satisfy the edge condition [10]. After the discretization of the space, the original field in the continuous space is approximated by a large number of line fields at the discretization points:

$$E_y(x, y, z, t) \rightarrow \left[E_{yk}(y, t)\right] = \left[E_{y1}, E_{y2}, \ldots, E_{yk}, \ldots, E_{yN_xN_z}\right]^t \quad (1)$$

0018-9480/90/1200-2051$01.00 ©1990 IEEE

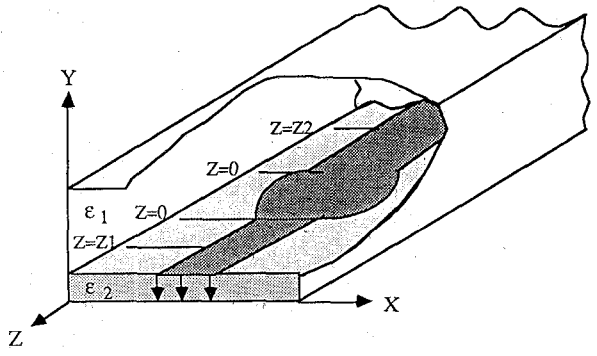

Fig. 1. A general planar transmission line with discontinuity in a shielded rectangular waveguide.

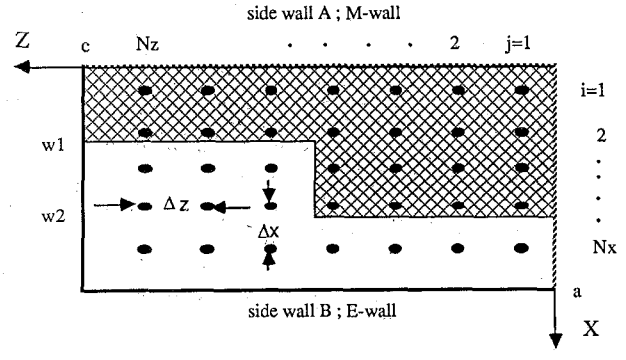

Fig. 2. Top view of the structure shown in Fig. 1 with the proper discretization points for the E_y component.

where

$$k = i + (j-1)N_x, \qquad 1 \leqslant i \leqslant N_x, \quad 1 \leqslant j \leqslant N_z.$$

B. Expansion of Input Pulse

In the structure shown in Fig. 1 with end walls, a field distribution at any time t, $[E_y(y,t)]$, can be expanded by modal field distributions, $[E_{yn}(y)]$, as follows:

$$\left[E_y(y,t)\right] = \sum_n \left(A_n \cos \omega_n t + B_n \sin \omega_n t\right)\left[E_{yn}(y)\right] \quad (2)$$

where [ ] denotes a column vector whose kth component represents the field value at the kth discretization line as shown in (1). Also the subscript n denotes the mode number. If the structure and the initial input support any static charge distribution, the dc mode ($\omega_n = 0$) should be included in (2) to obtain the correct time-domain data and frequency-domain information.

In the expansion (2), the coefficients A_n can be determined by the initial field distribution, $[E_y(y, t=0)]$, and the orthogonal property of the modal fields:

$$A_n = \frac{\int_0^b \left[E_y(y,t=0)\right]^t \left[E_{yn}(y)\right] dy}{\int_0^b \left[E_{yn}(y)\right]^t \left[E_{yn}(y)\right] dy}. \quad (3)$$

Also, the B_n can be found by the causality condition used in the time iteration method [11]:

$$B_n = A_n \tan(\omega_n \Delta t/2) \quad (4)$$

where

$$\Delta t \leqslant \min(\Delta x, \Delta z)/\left(C_{\max}\sqrt{3}\right) \quad (5)$$

and $C_{\max}$ is the maximum wave phase velocity within the structure.

In order to find the eigenfrequencies and modal field distributions of the structure, we borrow the technique used in the frequency-domain method of lines [12]. In this technique, the characteristic equation is obtained from the application of the metallic boundary condition to the metal strip on the dielectric interface boundary. The equation is given by (see the Appendix for details)

$$\begin{bmatrix}[E_z]\\ [E_x]\end{bmatrix}_{\text{red}} = \begin{bmatrix}[G_z]\\ [G_x]\end{bmatrix}_{\text{red}} [\rho]_{\text{red}} = [0] \qquad \text{for static fields} \quad (6a)$$

$$\begin{bmatrix}[E_z]\\ [E_x]\end{bmatrix}_{\text{red}} = \begin{bmatrix}[Z_{zz}] & [Z_{zx}]\\ [Z_{xz}] & [z_{xx}]\end{bmatrix}_{\text{red}} \begin{bmatrix}[J_z]\\ [J_x]\end{bmatrix}_{\text{red}} = [0]$$

for time-harmonic fields. (6b)

In order to obtain a nontrivial solution of (6b),

$$\det[Z(\omega)]_{\text{red}} = 0 \qquad \text{for time-harmonic fields} \quad (7)$$

where the subscript "red" represents the reduced matrices corresponding to the discretization points on the metal strip.

After the eigenfrequencies are found, (6a) and (6b) can be used to obtain the charge distribution, $[\rho]^t$, and the current density distributions, $[[J_z], [J_x]]^t$. The modal field distributions, $[E_{yn}(y)]$, can be derived from these quantities. It is found that (6a) and (6b) need to be solved by the QR method [13] to ensure stability of the results.

C. Time-Domain Data and Frequency-Domain Characteristics

Once procedures described above in subsections A and B are carried out, all the constants in (2) are determined so that the behavior of the input pulse at any point at any time can be calculated. Therefore, the characteristics of a circuit can be obtained by observing the propagation and the scattering of the short initial pulse in the given circuit. In this paper, we tested four structures: uniform microstrip line and its three commonly encountered discontinuities (step-in-width, open-end, and gap).

1) Uniform Microstrip Line: In this case, the transfer function can be found by

$$\exp[-\gamma(\omega)(z_1+z_2)] = V_y(\omega, z=z_2)/V_y(\omega, z=z_1) \quad (8)$$

where

$$\gamma(\omega) = \alpha(\omega) + j\beta(\omega) = \text{propagation constant of the uniform microstrip line}$$

$$V_y(\omega, z=z_1) = \text{Fourier transform of}\left[V_y(t, z=z_1)\right] \text{at a fixed } x$$

and

$$V_y(\omega, z = z_2)$$

$$= \text{Fourier transform of} \left[V_y(t, z = z_2) \right] \text{at a fixed } x.$$

$V_y(t, z)$ is a traveling voltage wave defined as the line integral of E_y from the microstrip to the ground plane. Stable results can be obtained by using this choice of voltage definition for the calculation of the frequency-domain characteristics. Also, the effective dielectric constant can be derived from the calculated phase constant, β, by

$$\epsilon_{\text{eff}}(\omega) = \beta^2(\omega)/\omega^2\mu_0\epsilon_0. \tag{9}$$

The voltage–current definition is used for the characteristic impedance calculation:

$$Z(\omega) = V_y(\omega, z = z_1)/I_z(\omega, z = z_1) \tag{10}$$

where the traveling current wave is found by a line integral of the H field around the microstrip line at $z = z_1$.

2) Discontinuities: In order to obtain the frequency-dependent scattering parameters of the discontinuity, the incident wave, $E_{y,\text{inc}}$ and the reflected wave, $E_{y,\text{ref}}$, should be calculated at some point on the input observation plane, z_1, and the transmitted wave, $E_{y,\text{trs}}$, at the corresponding point on the output observation plane, z_2. Then, the power ratio S parameter is given by

$$S_{11}(\omega) = \left[V_{y,\text{ref}}(\omega, z_1)/V_{y,\text{inc}}(\omega, z_1) \right] \exp\{2\gamma_1(\omega) z_1\} \tag{11}$$

$$S_{21}(\omega) = \left[V_{y,\text{trs}}(\omega, z_2)\sqrt{Z_{01}(\omega)}\,/V_{y,\text{inc}}(\omega, z_2)\sqrt{Z_{02}(\omega)} \right] \exp\{\gamma_1(\omega) z_1 + \gamma_2(\omega) z_2\} \tag{12}$$

where $\gamma_1(\omega)$ and $\gamma_2(\omega)$ are the propagation constants of the uniform microstrip lines connected to each port of the discontinuity.

III. Results and Discussion

In this paper, we study four structures on alumina subtrate ($\epsilon_r = 9.6$, $h = 0.635$ or 0.7 mm) shielded by rectangular waveguide ($a = 2$, $b = 10$, and $c = 45$ mm). They are a uniform microstrip line and its discontinuities (step-in-width, open-end, and gap). In the calculation of the variation of the fields in the time domain, we have used the following numbers of discretization points:

number of discretized points in x direction
$= 20(\Delta x = 0.095$ mm)
number of discretized points in z direction
$= 100(\Delta z = 0.445$ mm)
number of modes = 20

Fig. 3 shows the pulse propagation along the uniform microstrip ($h = 0.635$, $W = 0.635$ mm) in the time domain. Fig. 4 shows the effective dielectric constant (ϵ_{eff}) obtained by using the Fourier transform of the time-domain data of a uniform microstrip line in a rectangular waveguide with two different widths. The results show that the narrow waveguide reduces the effective dielectric constant.

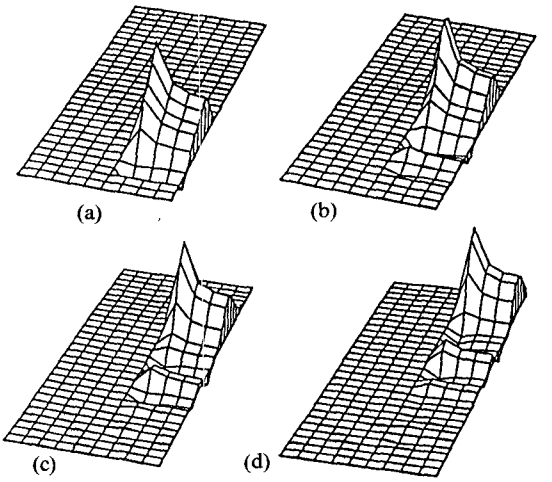

Fig. 3. E_y configuration beneath a uniform microstrip line ($a = 2$, $b = 10$, $h = 0.635$, $W = 0.635$ mm). (a) $t = 0$, (b) $t = 40$, (c) $t = 80$, and (d) $t = 120$ ps.

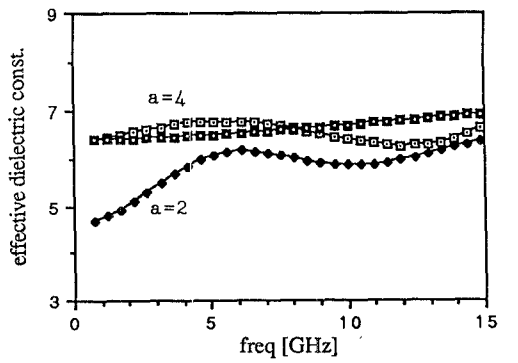

Fig. 4. Effective dielectric constant of the uniform microstrip line ($b = 10$, $h = 0.635$ [mm], $\epsilon_1 = 1$ and $\epsilon_2 = 9.6$) obtained by TDML: TDML curve-fit formula [1] (open structure).

Fig. 5 shows the characteristic impedance (Z_0) of a uniform microstrip line in a rectangular waveguide with two different widths. The results agree well with those from the closed-form formula given in [14] if the sidewall is sufficiently away from the edge of the microstrip line. However, the impedance is lowered by the sidewall if it is near the edge of the microstrip line.

Fig. 6 shows the scattering of the pulse at a microstrip step discontinuity in the time domain. Using (11) and (12), the frequency-domain characteristics can be extracted from the time-domain data. Fig. 7 shows the frequency-dependent scattering parameters of the given structure with the available published data [5].

Figs. 8 and 9 show the scattering of pulse at the microstrip ($h = 0.7$, $W = 0.7$ mm) open end and gap (s = 0.35 mm) in the time domain, respectively. The frequency-dependent scattering parameters derived from the time-domain data are shown in Figs. 10 and 11 with the FDTD results reported in [8]. They agree reasonably well with [8], although our results show some undulation due to the

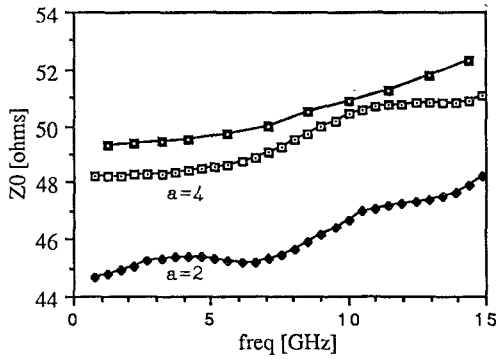

Fig. 5. Characteristic impedance for the uniform microstrip line shown in Fig. 3 ($b=10$, $h=0.635$ [mm], $\epsilon_1=1$ and $\epsilon_2=9.6$):

TDML curve-fit formula [1] (open structure).

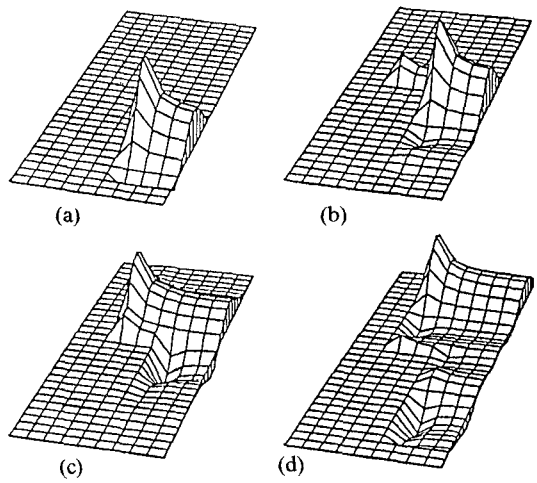

Fig. 6. E_y configuration beneath a microstrip step discontinuity ($a=2$, $b=10$, $W1=1.27$, $W2=0.635$ mm). (a) $t=0$, (b) $t=40$, (c) $t=80$, and (d) $t=120$ ps.

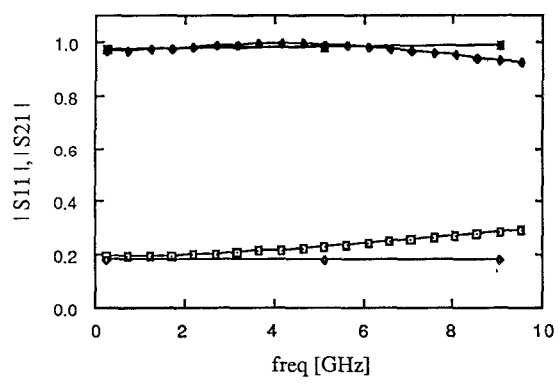

Fig. 7. Scattering parameters (S_{11}, S_{12}) for the symmetric step discontinuity shown in Fig 2($a=2$, $b=10$, $W1=0.3175$, $W2=0.635$ [mm], $\epsilon_1=1$ and $\epsilon_2=9.6$).

$S11$ $S21$ TDML $S11$ $S21$ ref. [5].

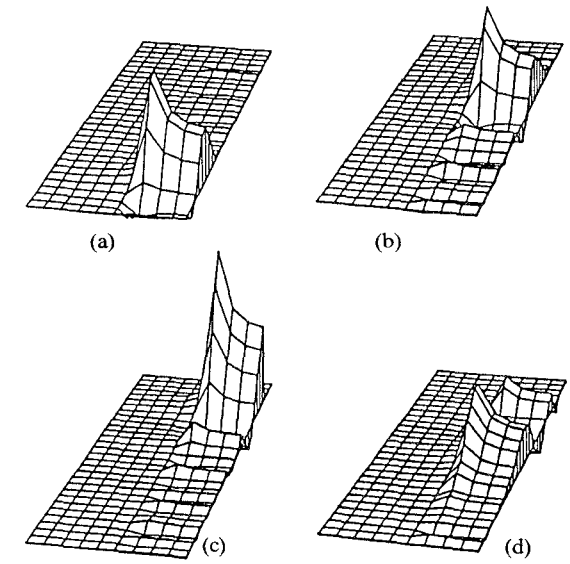

Fig. 8. E_y configuration beneath a microstrip open-end discontinuity ($a=2$, $b=10$, $W=0.7$ mm). (a) $t=0$, (b) $t=80$, (c) $t=120$, and (d) $t=200$ ps.

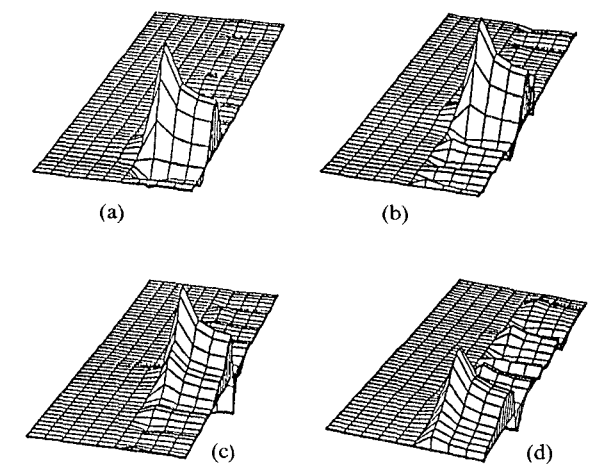

Fig. 9. E_y configuration beneath a microstrip gap discontinuity ($a=2$, $b=10$, $h=0.7$, $W=0.7$, and $s=0.35$ mm). (a) $t=0$, (b) $t=40$, (c) $t=80$, and (d) $t=120$ ps.

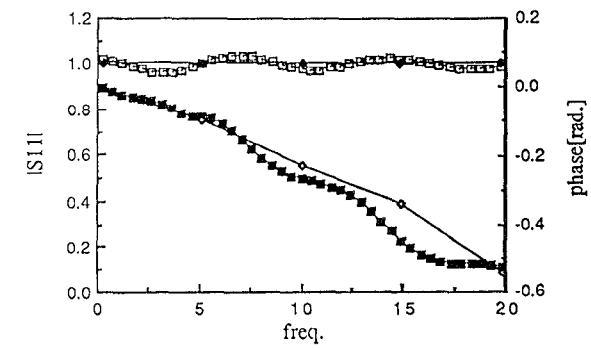

Fig. 10. The magnitude and phase of $S11$ for the microstrip open-end discontinuity:

mag phase present method mag phase [8].

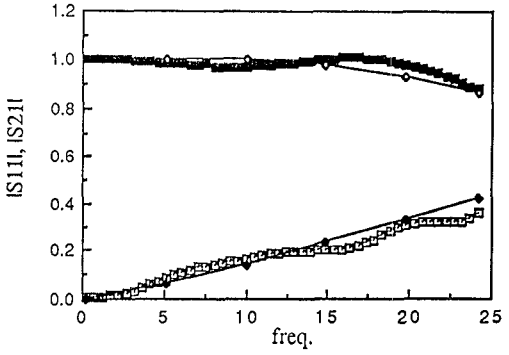

Fig. 11. The magnitudes of $S11$ and $S21$ for a microstrip gap discontinuity ($\epsilon_2 = 9.6$, $h = 0.7$ [mm], $W/h = 1$, and $s/h = 0.5$):
—□— $S21$ —◆— $S11$ present method —◆— $S21$ —◇— $S11$ [8].

discretization error and the truncation of the time-domain data [15]. It is believed that the error can be reduced by using a nonuniform discretization scheme and a proper window function in the FFT procedure.

IV. Conclusion

It has been demonstrated that the time-domain method of lines is a reliable and efficient method for dealing with pulse propagation and discontinuity problems in planar transmission lines. This is an extension of the two-dimensional results reported earlier. It was found that the dc mode should be included in the calculation to obtain the correct results and that the field can be described accurately by proper placement of the discretized E_y field points near the edge of the microstrip line. Also, the frequency-domain characteristics obtained from the time-domain data have been made more stable by applying the QR algorithm in the eigenmode determination and by using integrated field quantities in the extraction of frequency-domain parameters. The method can be applied to various planar structures.

Appendix

In the three-dimensional problem shown in Fig. 1, all six field components should be considered to satisfy the boundary conditions. Usually, two scalar potentials, $\Psi^e(x, y, z, t)$ and $\Psi^h(x, y, z, t)$, are introduced to simplify the formulation instead of considering all six field components. The fields can be derived from the solution of two scalar potentials. The equations for the potentials are given by

$$\partial^2\Psi^e/\partial x^2 + \partial^2\Psi^e/\partial y^2 + \partial^2\Psi^e/\partial z^2 - \mu\epsilon(y)\,\partial^2\Psi^e/\partial t^2 = 0 \tag{A1a}$$

$$\partial^2\Psi^h/\partial x^2 + \partial^2\Psi^h/\partial y^2 + \partial^2\Psi^h/\partial z^2 - \mu\epsilon(y)\,\partial^2\Psi^h/\partial t^2 = 0. \tag{A1b}$$

Using the separation of variables technique, $\Psi(x, y, z, t) = \psi(x, y, z)T(t)$, the time-dependent solution is of the form

$$T(t) = A\cos(\omega t) + B\sin(\omega t). \tag{A2}$$

The space-dependent equations are given by

$$\partial^2\psi^e/\partial x^2 + \partial^2\psi^e/\partial y^2 + \partial^2\psi^e/\partial z^2 + \omega^2\mu\epsilon(y)\psi^e = 0 \tag{A3a}$$

$$\partial^2\psi^h/\partial x^2 + \partial^2\psi^h/\partial y^2 + \partial^2\psi^h/\partial z^2 + \omega^2\mu\epsilon(y)\psi^h = 0. \tag{A3b}$$

After the discretization of the space as shown in Fig. 2, (A3a) and (A3b) can also be discretized:

$$\frac{\partial^2[\psi^e]}{\partial y^2} + \frac{[D_{xx}^{ND}][\psi^e]}{\Delta x^2} + \frac{[\psi^e][D_{xx}^{ND}]^t}{\Delta z^2} + \omega^2\mu\epsilon(y)[\psi^e] = [0] \tag{A4a}$$

$$\frac{\partial^2[\psi^h]}{\partial y^2} + \frac{[D_{xx}^{DN}][\psi^h]}{\Delta x^2} + \frac{[\psi^h][D_{xx}^{DN}]^t}{\Delta z^2} + \omega^2\mu\epsilon(y)[\psi^h] = [0] \tag{A4b}$$

where the matrices $[\psi^e]$ and $[\psi^h]$ are two-dimensional arrays whose ijth element represents the potential of the ijth line. The matrices $[D_{xx}^{ND}]$, $[D_{xx}^{DN}]$, $[D_{zz}^{ND}]$, and $[D_{zz}^{DN}]$ are the second order difference matrices incorporating the sidewall boundary conditions [12], [16].

Since the matrices $[D_{xx}^{ND}]$, $[D_{xx}^{DN}]$, $[D_{zz}^{ND}]$, and $[D_{zz}^{DN}]$ are real symmetric matrices, they can be diagonalized by appropriate transformation matrices. The potentials can also be transformed into the "transformed potentials."

$$[U] = [T_X^{ND}]^t[\psi^e][T_z^{ND}] \tag{A5a}$$

$$[V] = [T_X^{DN}]^t[\psi^h][T_Z^{DN}] \tag{A5b}$$

where the matrices $[T_x^{ND}]$ and $[T_z^{ND}]$ are the transformation matrices used for the diagonalization of the second-order difference matrices [12]. Then, (A4a) and (A4b) are transformed into

$$\frac{\partial^2[U]}{\partial y^2} + \frac{[d_{xx}^{ND}][U]}{\Delta x^2} + \frac{[U][d_{zz}^{ND}]^t}{\Delta z^2} + \omega^2\mu\epsilon(y)U = [0] \tag{A6a}$$

$$\frac{\partial^2[V]}{\partial y^2} + \frac{[d_{xx}^{DN}][V]}{\Delta x^2} + \frac{[V][d_{zz}^{DN}]^t}{\Delta z^2} + \omega^2\mu\epsilon(y)[V] = [0] \tag{A6b}$$

where $[d_{xx}^{ND}]$, $[d_{xx}^{DN}]$, $[d_{zz}^{ND}]$, and $[d_{zz}^{DN}]$ are the diagonalized matrices of the second-order difference matrices [12]. The boundary conditions are given in the transformed domain as follows:

$$[U] = 0 \quad \text{at } y = 0, b \tag{A7a}$$

$$\partial[V]/\partial y = 0 \quad \text{at } y = 0, b. \tag{A7b}$$

At $y=h$,

$$\frac{1}{j\omega\epsilon_r\epsilon_0}\frac{[d_x^{ND}][U_{\rm I}][d_z^{ND}]^t}{\Delta x\Delta z}-\frac{\partial[V_{\rm I}]}{\partial y}$$
$$-\frac{1}{j\omega\epsilon_0}\frac{[d_x^{ND}][U_{\rm II}][d_z^{ND}]^t}{\Delta x\Delta z}+\frac{\partial[V_{\rm II}]}{\partial y}=[0] \quad \text{(A7c)}$$

$$\frac{1}{j\omega\epsilon_r\epsilon_0}\left(\frac{[U_{\rm I}][d_{zz}^{ND}]^t}{\Delta z^2}+\omega^2\mu_0\epsilon_r\epsilon_0[U_{\rm I}]\right)$$
$$-\frac{1}{j\omega\epsilon_0}\left(\frac{[U_{\rm II}][d_{zz}^{ND}]^t}{\Delta z^2}+\omega^2\mu_0\epsilon_0[U_{\rm II}]\right)=[0] \quad \text{(A7d)}$$

$$\frac{1}{j\omega\mu_0}\frac{[d_x^{ND}]^t[V_{\rm I}][d_z^{ND}]}{\Delta x\Delta z}+\frac{\partial[U_{\rm I}]}{\partial y}$$
$$-\frac{1}{j\omega\mu_0}\frac{[d_x^{ND}]^t[V_{\rm II}][d_z^{ND}]}{\Delta x\Delta z}-\frac{\partial[U_{\rm II}]}{\partial y}=-[\tilde{J}_z] \quad \text{(A7e)}$$

$$\frac{1}{j\omega\mu_0}\left(\frac{[V_{\rm I}][d_{zz}^{DN}]^t}{\Delta z^2}+\omega^2\mu_0\epsilon_r\epsilon_0[V_{\rm I}]\right)$$
$$-\frac{1}{j\omega\mu_0}\left(\frac{[V_{\rm II}][d_{zz}^{DN}]^t}{\Delta z^2}+\omega^2\mu_0\epsilon_0[V_{\rm II}]\right)=[\tilde{J}_x] \quad \text{(A7f)}$$

where the subscript I and II in the potentials represent the two regions. The matrices $[d_x^{ND}]$ and $[d_z^{ND}]$ are the diagonalized matrices of the first-order difference matrices [12].

Notice that (A6a) and (A6b) are uncoupled. The general solution of the ijth line which satisfies the boundary conditions (A7a) and (A7b) can be obtained:

$$U_{{\rm I},ij}=A_{{\rm I},ij}\sinh\kappa_{{\rm I},ij}y \quad \text{(A8a)}$$
$$U_{{\rm II},ij}=A_{{\rm II},ij}\sinh\kappa_{{\rm II},ij}(b-y) \quad \text{(A8b)}$$
$$V_{{\rm I},ij}=B_{{\rm I},ij}\cosh\eta_{{\rm I},ij}y \quad \text{(A8c)}$$
$$V_{{\rm II},ij}=B_{{\rm I}_1,ij}\cosh\eta_{{\rm II},ij}(b-y) \quad \text{(A8d)}$$

where

$$\kappa_{{\rm I},ij}^2=-\left[d_{xx,i}^{ND}/\Delta x^2+d_{zz,j}^{ND}/\Delta z^2+\omega^2\mu\epsilon_r\epsilon_0\right] \quad \text{(A9a)}$$
$$\kappa_{{\rm II},ij}^2=-\left[d_{xx,i}^{ND}/\Delta x^2+d_{zz,j}^{ND}/\Delta z^2+\omega^2\mu\epsilon_0\right] \quad \text{(A9b)}$$
$$\eta_{{\rm I},ij}^2=-\left[d_{xx,i}^{DN}/\Delta x^2+d_{zz,j}^{DN}/\Delta z^2+\omega^2\mu\epsilon_r\epsilon_0\right] \quad \text{(A9c)}$$
$$\eta_{{\rm II},ij}^2=-\left[d_{xx,i}^{DN}/\Delta x^2+d_{zz,j}^{DN}/\Delta z^2+\omega^2\mu\epsilon_0\right]. \quad \text{(A9d)}$$

By means of these solutions, the derivatives of U and V with respect to y at $y=h$ can be represented by the values of U and V at $y=h$. Equations (A7c)–(A7f) have six unknowns: $U_{{\rm I},ij}$, $U_{{\rm II},ij}$, $V_{{\rm I},ij}$, $V_{{\rm II},ij}$, $J_{x,ij}$, and $J_{z,ij}$ at $y=h$. Therefore, the continuity equations in (A7c)–(A7f) can be used to solve for the potentials $U_{{\rm I},ij}$, $U_{{\rm II},ij}$, $V_{{\rm I},ij}$, and $V_{{\rm II},ij}$ at $y=h$ in terms of the current densities $J_{x,ij}$ and $J_{z,ij}$.

On the other hand, the filed values at $y=h$ can be found by using the following relations evaluated at $y=h$:

$$\widetilde{E_{x,ij}}(y)=\frac{1}{j\omega\epsilon(y)}\frac{d_{x,i}^{ND}d_{z,j}^{ND}}{\Delta x\Delta z}U_{ij}(y)$$
$$-\eta_{ij}\tanh\eta_{ij}hV_{ij}(y) \quad \text{(A10a)}$$

$$\widetilde{E_{y,ij}}(y)=\frac{1}{j\omega\epsilon(y)}\frac{d_{z,j}^{ND}}{\Delta z}\frac{\partial}{\partial y}U_{ij}(y)-\frac{d_{x,i}^{DN}}{\Delta x}V_{ij}(y) \quad \text{(A10b)}$$

$$\widetilde{E_{z,ij}}(y)=\frac{1}{j\omega\epsilon(y)}\left(\frac{d_{zz,j}^{ND}}{\Delta z^2}+\omega^2\mu\epsilon(y)\right)U_{ij}(y). \quad \text{(A10c)}$$

Equations (A10a) and (A10c) can be expressed in the following form:

$$\begin{bmatrix}[\widetilde{E_z}]\\ [\widetilde{E_x}]\end{bmatrix}=\begin{bmatrix}[\widetilde{Z_{zz}}] & [\widetilde{Z_{zx}}]\\ [\widetilde{Z_{xz}}] & [\widetilde{Z_{xx}}]\end{bmatrix}\begin{bmatrix}[\widetilde{J_z}]\\ [\widetilde{J_x}]\end{bmatrix} \quad \text{(A11)}$$

where the $[Z]$'s are diagonal matrices if the field and current matrices $[E_x]$, $[E_z]$, $[J_x]$, and $[J_z]$ are written in vector notation according to (1).

Now, the final boundary condition is that the tangential electric fields should be zero on the metal strip. In order to apply this condition, we need to go back to the original domain using the inverse transformation relation. Equation (A11) can be inverse transformed. Then, the reduced matrix can be obtained by deleting the rows and columns corresponding to the non-metallization lines from the full matrix:

$$\begin{bmatrix}[E_z]\\ [E_x]\end{bmatrix}_{\rm red}=\begin{bmatrix}[Z_{zz}] & [Z_{zx}]\\ [Z_{xz}] & [Z_{xx}]\end{bmatrix}_{\rm red}\begin{bmatrix}[J_z]\\ [J_x]\end{bmatrix}_{\rm red}=[0]. \quad \text{(A12)}$$

Equation (A12) will have nontrivial solutions at the resonant frequencies of the structure only. The resonant frequencies are found from the determinant equation

$$\det\begin{bmatrix}[Z_{zz}] & [Z_{zx}]\\ [Z_{xz}] & [Z_{xx}]\end{bmatrix}_{\rm red}=[0]. \quad \text{(A13)}$$

For the dc case, a similar procedure can be applied to the Poisson equation and the boundary conditions of electrostatic field to obtain (6a).

References

[1] K. C. Gupta, R. Garg, and I. J. Bahl, *Microstrip Lines and Slotlines*. Norwood, MA: Artech House, 1979, pp 41–104, 158–193

[2] J. R. James, and A. Henderson, "High-frequency behavior of microstrip open-circuit terminations," *Microwaves, Opt., Acoustics*, vol.3, pp. 205–218, Sept. 1979.

[3] P. B. Katehi, and N. G. Alexopoulos, "Frequency-dependent characteristics of microstrip discontinuities in millimeter-wave integrated circuits," *IEEE Trans Microwave Theory Tech.*, vol. MTT-33, pp. 1029–1035, Oct. 1985.

[4] R. W. Jackson and D. M. Pozar, "Full-wave analysis of microstrip open-end and gap discontinuities," *IEEE Trans Microwave Theory Tech.*, vol. MTT-33, pp. 1036–1042, Oct. 1985.

[5] N. H. L. Koster, and R. H. Jansen, "The microstrip step discontinuity: A revised description," *IEEE Trans. Microwave Theory Tech.*, vol. MTT-34, pp. 213–223, Feb. 1986.

[6] Y. C. Shih, and W. J. R. Hoefer, "Dominant and second-order mode cutoff frequencies in fin lines calculated with a two-dimen-

sional TLM program," *IEEE Trans. Microwave Theory Tech.*, vol. MTT-28 pp. 1443–1981, Dec. 1980.

[7] N. Yoshida, and I. Fukai, "Transient analysis of a stripline having a corner in three-dimensional space," *IEEE Trans Microwave Theory Tech.*, vol. MTT-32, pp. 491–498, May 1984.

[8] X. Zhang and K. K. Mei, "Time-Domain finite difference approach for the calculation of the frequency-dependent characteristics of the microstrip discontinuities," *IEEE Trans Microwave theory Tech.*, vol. 36, pp. 1775–1787, Dec. 1988

[9] S. Nam, S. El-Ghazaly, H. Ling and T. Itoh, "Time-domain method of lines applied to a partially filled waveguide," in 1988 *IEEE MTT-S Int. Microwave Symp. Dig.* pp. 627–630.

[10] U. Schulz, "On the edge condition with the method of lines in planar waveguide," *Arch. Elek. Ubertragung.* pp. 176–178, 1980.

[11] A. Taflove, and K. R. Umashanker,, "The finite-difference time-domain method for electromagnetic scattering and interaction problems" *JEWA.*, vol. 1, no. 3, pp. 243–267, 1987.

[12] S. G. Worm and R. Pregla, "Hybrid-mode analysis of arbitrarily shaped planar microwave structures by the method of lines," *IEEE Trans. Microwave Theory Tech.*, vol. MTT-32, pp. 191–196, 1984.

[13] "The IMSL Library," IMSL Inc., Edition 9.2, subroutine LLSQF, 1984.

[14] T. C. Edwards, *Foundations for Microstrip Circuit Design*, New York: Wiley, 1981, pp. 74–77

[15] C. T. Chen, *One-Dimensional Digital Signal Processing* New York: Marcel Dekker, pp. 110–116.

[16] S. Nam, "A study of a new time-domain method of lines and its application for the characterization of microstrip line and its discontinuities," Ph.D. dissertation, University of Texas at Austin, 1989.

✠

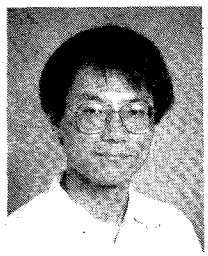

S. Nam was born in Korea on February 2, 1959. He received the B.S. degree in electronic engineering from the Seoul National University in 1981, the M.S. degree in electrical engineering from the Korea Advanced Institute of Science and Technology in 1983, and the Ph.D. degree in electrical engineering from the University of Texas at Austin in May 1989. He is a postdoctoral fellow at the Electrical Engineering Research Laboratory at the University of Texas at Austin. His research interests are in the area of microwave fields and circuits, in particular guided wave structures and their discontinuity effects on microwave circuits.

✠

Hao Ling (S'83–M'86) was born in Taichung, Taiwan, on September 26, 1959. He received the B.S. degrees in electrical engineering and physics from the Massachusetts Institute of Technology in 1982, and the M.S. and Ph.D. degrees in electrical engineering from the University of Illinois at Urbana-Champaign in 1983 and 1986, respectively.

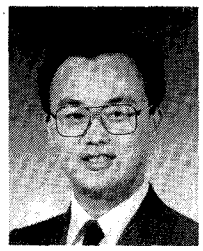

In 1982, he was associated with the IBM Thomas J. Watson Research Center. Yorktown Heights, NY, where he conducted low-temperature experiments in the Josephson Department. While in graduate school at the University of Illinois, he held a research assistantship in the Electromagnetics Laboratory as well as a Schlumberger Fellowship. In 1986, he joined the Department of Electrical and Computer Engineering at the University of Texas at Austin as an Assistant Professor. He participated in the Summer Visiting Faculty Program in 1987 at the Lawrence Livermore National Laboratory. His current research interests include radar cross section analysis of partially open cavities and the characterization of microstrip discontinuities.

Dr. Ling was a recipient of the 1987 National Science Foundation Presidential Young Investigator Award.

✠

Tatsuo Itoh (S'69–M'69–SM'74–F'82) received the Ph.D. degree in electrical engineering from the University of Illinois. Urbana, in 1969.

From September 1966 to April 1976, he was with the Electrical Engineering Department. University of Illinois. From April 1976 to August 1977, he was a Senior Research Engineer in the Radio Physics Laboratory, SRI International, Menlo Park, CA. From August 1977 to June 1978, he was an Associate Professor at the University of Kentucky, Lexington. In July 1978, he joined the faculty at the University of Texas at Austin, where he is now a Professor of Electrical Engineering and Director of the Electrical Engineering Research Laboratory. During the summer of 1979, he was a guest researcher at AEG-Telefunken, Ulm West Germany. Since September 1983, he has held the Hayden Head Centennial Professorship of Engineering at the University of Texas. In September 1984, he was appointed Associate Chairman for Research and Planning of the Electrical and Computer Engineering Department. He also holds an Honorary Visiting Professorship at the Nanjing Institute of Technology, China.

Dr. Itoh is a member of Sigma Xi and of the Institute of Electronics and Communication Engineers of Japan. He is a member of Commission B and Chairman of Commission D of USNC/URSI. He served as the Editor of the IEEE TRANSACTIONS ON MICROWAVE THEORY AND TECHNIQUES for the years 1983–1985. He serves on the Administrative Committee of the IEEE Microwave Theory and Techniques Society. Dr. Itoh is a Professional Engineer registered in the state of Texas.